The inside-out planetary nebula around a born-again star

Martín A. Guerrero[1], Xuan Fang[2], Marcelo M. Miller Bertolami[3,4], Gerardo Ramos-Larios[5], Helge Todt[6], Alexandre Alarie[7], Laurence Sabin[7], Luis F. Miranda[1], Christophe Morisset[7], Carolina Kehrig[1], and Saúl A. Zavala[8]

[1] Instituto de Astrofísica de Andalucía, IAA-CSIC, Granada, Spain
[2] Laboratory for Space Research & Department of Physics, Faculty of Science, The University of Hong Kong, Hong Kong, People's Republic of China
[3] Instituto de Astrofísica de La Plata, UNLP-CONICET, La Plata, Argentina
[4] Facultad de Ciencias Astronómicas y Geofísicas, UNLP, La Plata, Argentina
[5] Instituto de Astronomía y Meteorología (IAM), Dept. de Física, CUCEI, Universidad de Guadalajara, Guadalajara, Jalisco, Mexico
[6] Institute of Physics and Astronomy, University of Potsdam, Potsdam, Germany
[7] Instituto de Astronomía, Universidad Nacional Autónoma de México, Ensenada, B.C., Mexico
[8] Tecnológico Nacional de México/I.T. Ensenada, Departamento de Ciencias Básicas, Ensenada, B.C., Mexico.

Planetary nebulae are ionized clouds of gas formed by the hydrogen-rich envelopes of low- and intermediate-mass stars ejected at late evolutionary stages. The strong UV flux from their central stars causes a highly stratified ionization structure, with species of higher ionization potential closer to the star. Here we report on the exceptional case of HuBi 1, a double-shell planetary nebula whose inner shell presents emission from low-ionization species close to the star and emission from high-ionization species farther away. Spectral analysis demonstrates that the inner shell of HuBi 1 is excited by shocks, whereas its outer shell is recombining. The anomalous excitation of these shells can be traced to its low-temperature [WC10] central star whose optical brightness has declined continuously by 10 magnitudes in a period of 46 years. Evolutionary models reveal that this star is the descendent of a low-mass star ($\simeq 1.1$ $M_\odot$) that has experienced a born-again event[1] whose ejecta shock-excite the inner shell. HuBi 1 represents the missing link in the formation of metal-rich central stars of planetary nebulae from low-mass progenitors, offering unique insight regarding the future evolution of the born-again Sakurai's object[2]. Coming from a solar-mass progenitor, HuBi 1 represents a potential end-state for our Sun.

Planetary nebulae (PNe) are a short-lived ≈20,000 yr period in the transition of low- and intermediate-mass stars ($M_{initial} = 0.8 - 8.0 M_\odot$) from the Asymptotic Giant Branch (AGB) phase towards the white-dwarf (WD) phase. The ionization structure of PNe,

governed by the distance of the nebular material to the central star (CSPN), is well-known to display an onion-like structure with higher ionization species such as He^{++} and O^{++} close to the central star, lower ionization species such as N^+ and O^+ in the outer region, and neutral and molecular species such as O^0 and H_2 in the outermost photo-dissociation region.

Whereas this is the general rule, we have discovered an exceptional case in HuBi 1[3] (PN G012.2+04.9, a.k.a. PM 1-188). Originally reported to have a faint bipolar outer shell and an unresolved bright inner shell[4], our sub-arcsec resolution images (Figure 1a) and spatial profiles of selected emission lines (Figure 1b-d) extracted from sub-arcsec long-slit spectroscopic observations refine this description, while unveiling a puzzling fact: the outer shell of HuBi 1, a barrel-like structure with faint polar protrusions slightly inclined to the line of sight (see Methods), surrounds a [N II]-bright inner shell (Figure 1b). The low-excitation inner shell of HuBi 1 is unusual among PNe, but its ionization structure is even more peculiar (Figure 1c,d). The spatial profile of the [O II] $\lambda 3727$ emission line fills the inner shell cavity whose rim is defined by the [N II] $\lambda 6548$ and [O III] $\lambda 5007$ emission lines. This is exactly opposite to typical photo-ionized nebulae, where the [N II] and [O II] spatial profiles are generally coincident with each other and the [O III] profile peaks inside, given the very similar ionization potentials required for O^+ and N^+ and the higher ionization potential for O^{++}. More surprisingly, perhaps, the spatial profile of the He II $\lambda 4686$ line peaks outside those of [N II] and [O III], although the ionization potential for He^{++} is higher than for N^+ and O^{++}. The ionization structure of the inner shell of HuBi 1 is inverted with respect to that of photo-ionized nebulae. In this sense, HuBi 1 is inside-out.

The origin of the inverted ionization structure of the inner shell of HuBi 1 must be at its CSPN, IRAS 17514-1555 (hereafter IRAS 17514). This star is of [WR]-type, i.e. its spectrum shows relatively broad emission lines similar to those of massive Wolf-Rayet (WR) stars[5] that indicate H-deficient strong stellar winds. The spectrum of IRAS 17514, which reveals a wealth of C II and C III emission lines[4] arising from a C-rich stellar wind, has been assigned a spectral type of [WC10][6]. Our analysis of mid-1990s spectroscopic observations of IRAS 17514 using state-of-the-art non-LTE models (see Methods) confirms its low terminal wind velocity $v_\infty \approx 360$ km s^{-1}, low surface temperature $T_\star \approx 38,000$ K, and high C and O abundances[7]. The number of He^+ ionizing photons suggested by this non-LTE stellar model, $\log Q$(He II)<34, is much lower than that derived for the nebula, $\log Q$(He II)>43.8 (see Methods). Not only is the spatial distribution of the He II emission in HuBi 1 unexpected for a photo-ionized nebula, but its detection is puzzling because the CSPN is not hot enough to photo-ionize He^+.

The actual state of affairs is more complex yet. A revision of long-term optical photometry and spectroscopy of IRAS 17514 (see Methods) reveals it has faded continuously over time (Figure 2). Back to March 1989, the star had a V-band magnitude of 14.6, which faded

to 19.8 in June 2014, and was above a detection limit $\geq$22.7 in May 2017. Using archival USNO B-1 data obtained on January 1971, we found a decline in the B and R bands by nearly 10 mags, implying a decrease in optical brightness $\cong$10,000 times in 46 years. The spectral changes in IRAS 17514 during the period from 1996 to 2014 are mainly restricted to its stellar continuum, as the profiles and equivalent widths of the spectral lines remained unchanged. Since spectral lines are very sensitive to $T_\star$, a change of $T_\star > 2,000$ K can be discarded. Such small variation in $T_\star$ would imply a tiny change in the optical flux, which depends almost linearly on $T_\star$ given that the optical region of a CSPN spectrum can be approximated with the Rayleigh-Jeans Law. Rather, the decline in time of the optical flux of IRAS 17514 is associated with a correlated increase in obscuration.

At the present time, IRAS 17514 cannot even provide the ionizing flux required to keep hydrogen ionized in HuBi 1, which is estimated to be $\log Q(\text{H \textsc{i}})$=45.7. With such a rapidly fading CSPN, the nebula is expected to exhibit unusual spectral properties. Indeed, the spectra of the inner and outer shells have their own share of peculiarities (see Methods). The outer shell is dominated by H \textsc{i} and He \textsc{i} recombination lines, with much fainter emission of forbidden lines, which is reminiscent of recombining haloes in PNe[8]. MAPPINGS photo-ionization models following the time-evolution of a low-density photo-ionized PN after the ionizing UV flux from its CSPN ceases show that its cooling time-scale is only a few decades, whereas its recombination time-scale is much longer, several thousand years (see Methods). As for the inner shell, the brightest emission lines in its spectrum are those of [N \textsc{ii}], with the notable detection of the He \textsc{ii} line at 4686 Å. The inverted ionization structure and spectrum of this shell are typical of shocks propagating through an ionized medium[9]. Indeed, where the CLOUDY photo-ionization models using the best-fit non-LTE stellar atmosphere model of IRAS 17514 fail to reproduce those, MAPPINGS models including shock excitation are successful for shock velocities $\gtrsim$70 km s^{-1} (see Methods). As the shock travels outwards through the ionized outer shell of HuBi 1, He \textsc{ii} emission arises at the location of the shock, while the [O \textsc{ii}], [O \textsc{iii}], and [N \textsc{ii}] emissions at the post-shock cooling region.

Therefore, HuBi 1 is a fossil nebula surrounding a shock-excited inner shell. Its CSPN, IRAS 17514, has recently started ejecting large amounts of carbon-rich material at speeds faster than the nebular expansion. The expansion of this ejecta shock-excites the inner shell and, as it streams away, it cools down to conditions optimal for condensation of dust grains[10]. The increasing optical depth of the dusty circumstellar cocoon shields the UV photons from the CSPN, so that the outer nebula cools down and has started recombining.

Obviously, this is not the classical behavior for a CSPN. Dramatic drops in luminosity have been observed in slow novae[11] and R CrB stars[12], but the spectral properties and variation timescale of these sources differ from those of IRAS 17514. The C-rich dense stellar winds of (truly massive) WC stars provide suitable sites for dust production[13], either in episodic WC dust makers associated with eccentric binary systems with colliding

winds (CWB) or persistent WC dust makers (WCd). We note that the photometric behavior of WCd stars, with short (days to weeks) episodes of diminished brightness up to a few magnitudes[14] does not fit that of HuBi 1.

The key to understanding HuBi 1 is the [WC] nature of its CSPN. [WC]-type central stars account for a non-negligible fraction (∼15%) of CSPNe[15], but their origin is still debated. It has been proposed that they form through a thermal pulse, either at the end of the AGB (a final thermal pulse, FTP), during the post-AGB evolution of the CSPN when H-burning is still active (a late thermal pulse, LTP[16]), or early in the cooling phase of the WD evolution (a very late thermal pulse, VLTP[17]). These different channels result in different size and density of the PN, as well as distinct chemical composition of the CSPN. An FTP will result in a dense and dusty nebula with bright IR emission around the [WC] star, which has been suggested for the IR-[WC] class[18]. The old kinematical age and low density of the outer shell of HuBi 1 (≈9,000 years and ≈200 cm^{-3}, respectively, see Methods) rather favor a VLTP. Born-again events such as V605 Aql, V4334 Sgr (a.k.a., the Sakurai's object), and FG Sge imply notable stellar temperature variations in short (a few years[1, 2]) timescales and even faster drops in luminosity, within days or weeks; but these are not observed in IRAS 17514. *Ad-hoc* late stellar evolution models following VLTP events of low-mass progenitors reveal loops in the HR diagram resulting in extended phases of stalled T_{eff} (see Methods). The observed properties of HuBi 1 (kinematical age) and its CSPN (luminosity, surface temperature in the 1996-2014 period, and stellar wind abundances) can be reproduced with a VLTP in a 1.1 $M_{\odot}$ progenitor (Figure 3).

IRAS 17514 is caught in a brief but key episode in the evolution of a [WC] star and the nebula around it, which can be described by a low-mass born-again event. The ejecta associated with this VLTP is propagating a shock through the surrounding outer shell of HuBi 1 resulting in an inner shell with an inverted ionization structure unequaled among PNe, while its kinetic energy and significant enrichment in metals provide a direct clue to understanding the high turbulence of PNe around [WC]-type nuclei[19] and their higher C and N abundances[20]. IRAS 17514 provides the missing link between born-again events in low-mass stars like V4334 Sgr[2] and fully developed [WC]-nuclei, leaving open the possibility for our Sun itself, once it has become a PN[21], to experience a born-again event and conclude its life as a H-poor CSPN. The rapid evolution of HuBi 1 and its CSPN deserves close monitoring. The possible expansion of its inner shell, continuous dust production around the CSPN or its surface temperature increase can provide crucial insights to the formation of [WC] stars and deposition of energy and enriched material in the surrounding PNe.
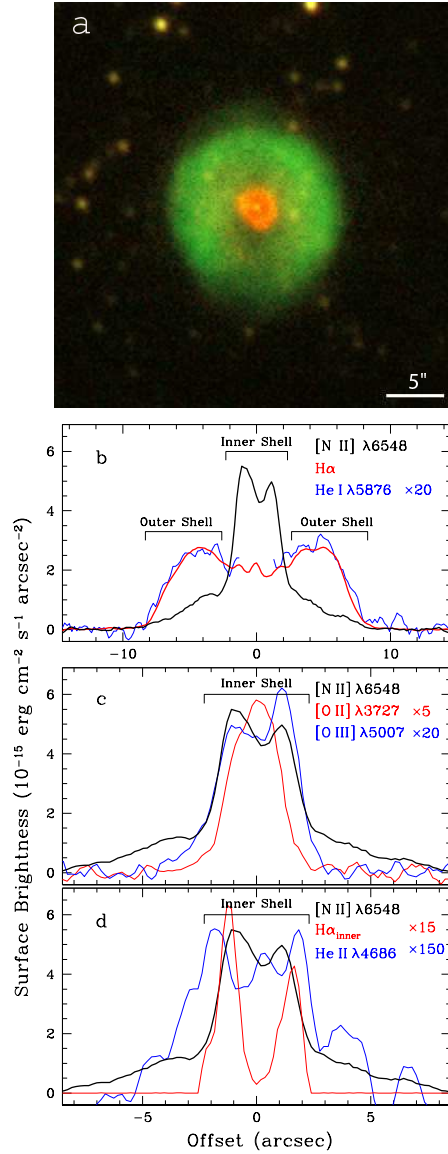
Figure 1.– Color composite picture and spatial profiles of selected lines of HuBi 1. (a) NOT ALFOSC [N II] $\lambda6584$ (red) and Hα $\lambda6563$ (green) color composite picture of HuBi 1. Hα emission dominates the $18\overset{''}{.}4 \times 19\overset{''}{.}2$ outer shell, whereas the $\simeq 4''$ inner shell is brighter in [N II]. (b-d) Continuum-subtracted spatial profiles of nebular emission lines (see Methods) along the East-West direction of HuBi 1 across its central star for the outer (b) and inner shells (c-d). The Hα spatial profile of the inner shell in panel d is computed by subtracting to the total Hα emission profile in panel b a model for the emission from the outer shell (see Methods). The extent of the inner and outer shells, as used to extract one-dimensional spectra, is marked.

5
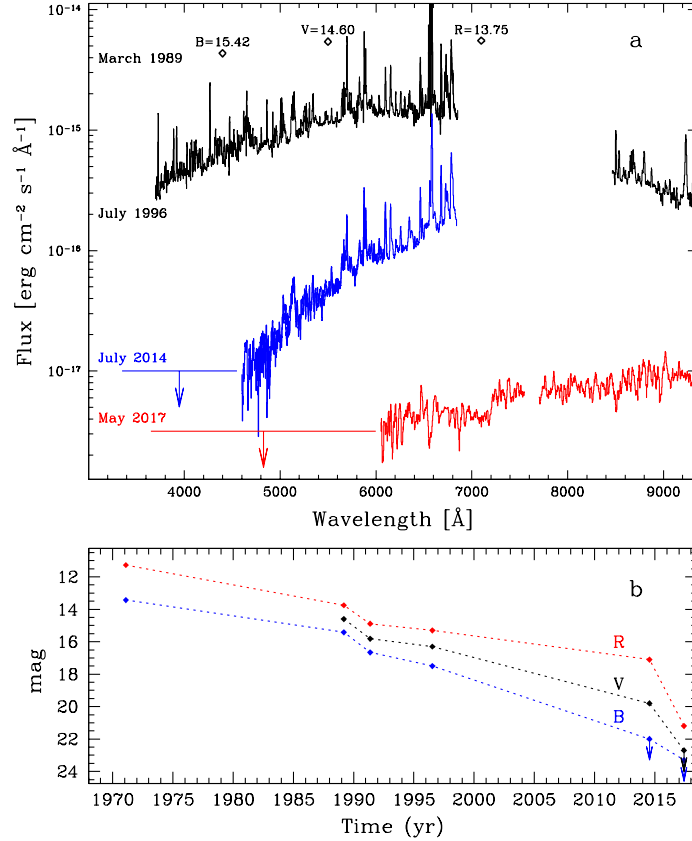
Figure 2.– Long-term spectro-photometric evolution of IRAS 17514-1555, the central star of HuBi 1. (a) Optical spectra obtained at different epochs between July 1996 and May 2017. The March 1989 BVR magnitudes of the discovery paper of HuBi 1[3] are included for reference. The horizontal lines and down-pointing arrows indicate detection upper limits. (b) Time evolution of the BVR magnitudes of IRAS 17514 as derived from photometric or spectroscopic measurements.
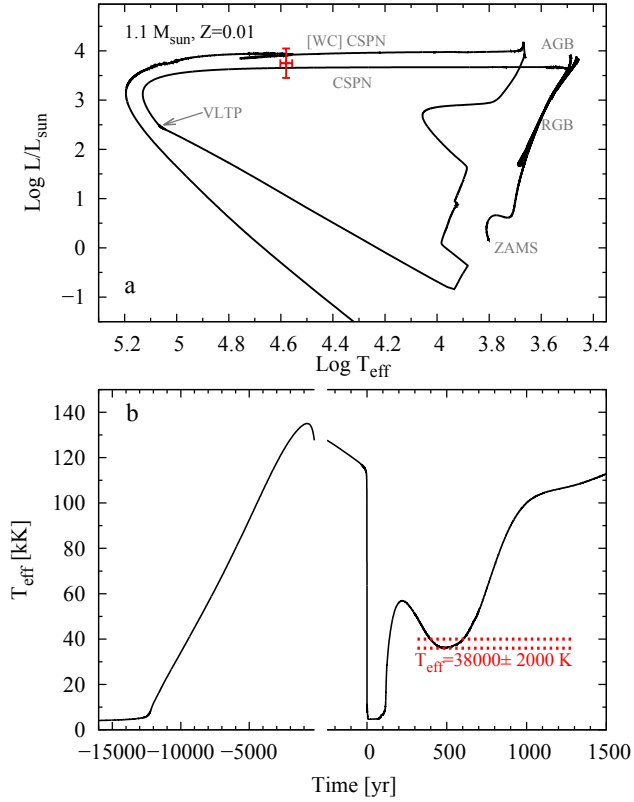
Figure 3.– **Evolutionary sequence of a PN progenitor with initial mass 1.1 $M_{\odot}$ that experiences a VLTP** (see Methods for additional details). (a) Evolutionary track in the HR diagram. The post-AGB star has a mass of 0.551 $M_{\odot}$. The red cross indicates the current location (with uncertainties) of HuBi 1 CSPN. (b) Post-AGB time evolution of T_{eff}. The time origin in this plot is set at the moment of the VLTP event, with different time scales being used before and after it. Note that the star departed from the AGB phase $\approx$12,000 yr before the occurrence of the VLTP, as marked by the initial increase of T_{eff} in this plot. The red-dotted lines mark the uncertainty in the temperature of the central star of HuBi 1, which is constrained by the ionization balance of the carbon and silicon ions as derived from the observed relative line strengths of C II, C III, and C IV lines, and Si III and Si IV lines (see Methods for further details).

7

Methods

Optical image of HuBi 1. Optical images of HuBi 1 were obtained on September 2, 2008, using the ALhambra Faint Object Spectrograph and Camera (ALFOSC) at the 2.5m Nordic Optical Telescope (NOT) of the Observatorio de El Roque de los Muchachos (ORM, La Palma, Spain). The EEV 2K×2K CCD camera was used, providing a pixel scale of $0.184''$ pix^{-1} and a field-of-view (FoV) of $6.3'$. Two 600s exposures were obtained through narrow-band filters that isolate the [N II] $\lambda6584$ and Hα $\lambda6563$ emission lines. These individual exposures were bias subtracted and flat-fielded using appropriate twilight sky frames, and then aligned and combined using standard IRAF routines. The spatial resolution of the images, as derived from stars in the FoV, is $0.65''$. The images were combined into the color picture shown in Figure 1a to highlight the different spatial locations of the Hα recombination and low-ionization [N II] lines.

Spatial profiles of selected emission lines of HuBi 1. Long-slit optical spectra of HuBi 1 were obtained on July 20, 2014 using also ALFOSC at the 2.5m NOT telescope. The 600 lines mm^{-1} #7 and #14 grisms were used to acquire two 1,200s exposures in the red and blue regions of the optical spectrum, respectively, covering the spectral range from 3250 to 6840 Å at a spectral resolution of 5.8 Å. The slit was placed at the central star along the East-West direction, i.e. at a position angle (PA) of $90°$. The spectro-photometric standard stars BD+33°2642 and BD+28°4211 were used for flux calibration. The seeing during the observations was $0.85''$, as determined from the FWHM of the continuum of field stars covered by the slit.

The two-dimensional spectra were used to extract spatial profiles of emission lines of interest along the long-slit, i.e., along the East-West direction across the central star. These spatial profiles were continuum subtracted using contiguous spectral regions free from emission lines. The emission line spatial profiles are 6 to 8 Å wide, whereas the redwards and bluewards contiguous background spatial profiles add together a width of 48 Å. Since the flux from the emission line is integrated and divided by the long-slit width and pixel scale, the resulting spatial profile represents the surface brightness of the nebula along this direction. Note that the [N II] $\lambda6548$ line is used for the [N II] spatial profile instead of the three times brighter [N II] $\lambda6584$ line because the latter is contaminated by bright stellar C II $\lambda\lambda6578,6582$ emission lines.

These profiles are shown in Figure 1b-d. Panel *b* shows the [N II] $\lambda6548$, Hα $\lambda6563$, and He I $\lambda5876$ emission lines, the latter multiplied by 20. The spatial profiles of the Hα and He I lines are similar and reveal the location of the outer shell. The spatial profile of the [N II] line peaks inside and reveals the location of the inner shell. The inner shell is shown into more detail in panels *c* and *d* of Figure 1. Panel *d* reveals that the spatial profile of the He II $\lambda4686$ line extends outside that of the [N II] $\lambda6548$ line, whereas the Hα inner shell synthetic profile peaks between those of He II and [N II]. This synthetic inner shell Hα spatial profile was obtained after subtracting to the observed Hα spatial profile in

8

panel *b* a two-Gaussian fit that represents the emission from the outer shell.

Age and morpho-kinematic modeling of the outer shell of HuBi 1. Long-slit, high-resolution spectra of HuBi 1 were obtained with the Manchester Echelle Spectrograph (MES) attached to the 2.1m telescope of the OAN-SPM Observatory. Four 1800s spectra were obtained on 2015 August 14 and 15 with the slit oriented East-West (PA=90°), and three 1800s spectra on 2018 May 5 with the slit oriented North-South (PA=0°). In both cases, the slit was placed across the CSPN and the detector was a 2K×2K E2V CCD in a 2×2 on-chip binning, leading to a dispersion of 0.057 Å pix^{-1} and a spatial scale of 0.35″ pix^{-1}. The slit length is 6.′5 and its width was set to 1″. A $\Delta\lambda = 90$ Å bandwidth filter was used to isolate the 87th order covering the Hα and [N II] $\lambda\lambda$6548,6584 emission lines. A ThAr arc lamp was used for wavelength calibration to an accuracy of 1 km s^{-1}. The spectral resolution is 12 km s^{-1}, as indicated by the $FWHM$ of the ThAr arc lines. The seeing was 1.2″–1.5″ during the observations.
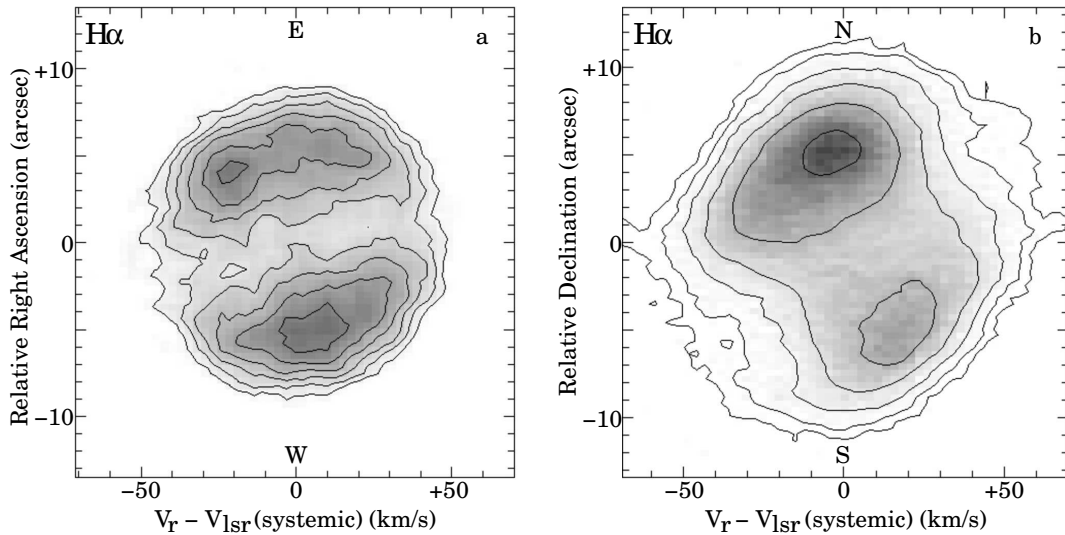

Supplementary Figure 1.– Position-velocity (PV) maps of the Hα emission line from the outer shell of HuBi 1 as observed through a long-slit placed on the CSPN at PA 90° (a) and PA 0° (b). The line intensity is shown in grey-scale and contours. The spatial origin corresponds to the position of the CSPN, whereas the radial velocities are relative to the systemic velocity of the nebula of +64.8 km s^{-1} as measured in the local standard of rest (LSR).

The spectra at each PA were combined into a single long-slit spectrum. The position-velocity (PV) maps of the Hα emission line from the outer shell are shown in the Supplementary Figure 1. The Hα emission line in the PV map at PA 90° appears as a velocity ellipse, although the detailed distribution of the emission in this map, with faint emission at high velocity at the nebular center, is not completely consistent with a spherical shell. Indeed, the open tilted line emission in the PV map at PA 0° is suggestive of an elongated

9

open-ended structure slightly tilted with respect to the line of sight.

To reproduce the observed Hα PV maps and image of HuBi 1, we have used the three-dimensional morpho-kinematic code SHAPE[28]. A barrel-like structure with fainter polar protrusions tilted with respect to the line of sight has been adopted to reproduce the general morphologies of the Hα PV maps and image. A satisfactory fit is achieved with a barrel-like structure with aspect ratio $\gtrsim 1.0$ whose symmetry axis is tilted to the line of sight by $\approx 25°$. Adopting a distance of 5.3 kpc[25], the kinematical age of the outer shell of HuBi 1 is found to be $\approx 9,000$ yr.

Non-LTE model of IRAS 17514. Archival Isaac Newton Telescope (INT) Intermediate-Dispersion Spectrograph (IDS) optical spectra of IRAS 17514 (July 1996) were analyzed using the Potsdam Wolf-Rayet (PoWR) model atmosphere code. PoWR is a state-of-the-art non-LTE radiative transfer code that accounts for mass-loss, line-blanketing, and wind clumping[22]. It can be applied to a wide range of hot stars of arbitrary metallicities[23, 24] with different luminosity L, stellar temperature $T_\star$, surface gravity $g_\star$, and mass-loss rate $\dot{M}$.
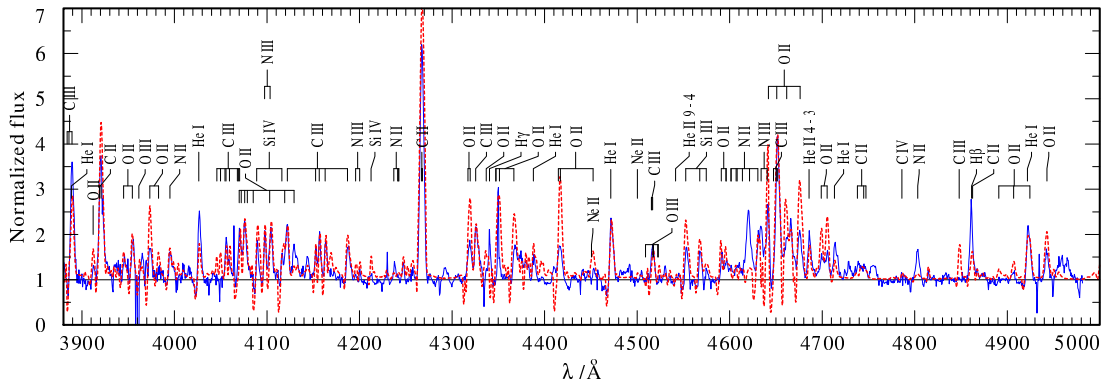
Supplementary Figure 2.– Optical spectrum of IRAS 17514 (blue) superimposed by the best-fit PoWR model (red). The identifications of key lines are labeled.

Initial stellar parameters[7] were refined on the basis of improved atomic data and line-blanket models including complex model atoms for H, He, C, N, O, Ne, Si and the iron group elements Sc, Ti, V, Cr, Mn, Fe, Co, and Ni. A temperature of 38,000±2,000 K is determined from the observed relative line strengths of C II $\lambda\lambda 4266.9, 4267.9$, C III $\lambda 5695.9$, and C IV $\lambda\lambda 5801.3, 5812.0$, and those of Si III $\lambda\lambda 4552.6, 4567.8, 4574.8$, and Si IV $\lambda\lambda 4088.8$ 4116.1. For a temperature of 36,000 K, the C III and C IV lines become much weaker in the model than in the observation, and the predicted Si III to Si IV line ratio becomes higher than observed. On the other hand, for a temperature of 40,000 K, the C III, C IV, and Si IV lines in the model become too strong, whereas the C II and Si III lines appear too weak. In this best-fit model, shown in the Supplementary Figure 2, the luminosity $\log(L/L_\odot)$ is 3.8±0.3, the extinction E_{B-V} 1.50±0.05 mag, the stellar radius 1.8 $R_\odot$, the

terminal wind velocity v_∞ 360±30 km s^{-1}, and the mass-loss rate $\approx$8×10^{-7} $M_\odot$ yr^{-1}. The chemical abundances by mass fraction are 0.01–0.05 for hydrogen, 0.33±0.10 for helium, and 0.5±0.1 for carbon, whereas rough estimates of 0.01 for nitrogen, 0.1 for oxygen, 0.04 for neon, and 0.01 for silicon are obtained. Solar abundances of 1.4×10^{-3} were adopted for iron.

H I and He II ionizing flux. The H I and He II ionizing flux can be derived from the intrinsic luminosity of the Hα λ6563 and He II λ4686 emission lines using the relations:
$Q(\text{H I}) = L_{\text{H}\alpha}/[j(\text{H}\alpha)/\alpha_\text{B}(\text{H I})]$,
$Q(\text{He II}) = L_{\text{He II } \lambda4686}/[j(\text{He II } \lambda4686)/\alpha_\text{B}(\text{He II})]$,
assuming case B recombination and $T_e = 10,000$ K in the low density case for the emission j and recombination α coefficients. Assuming that the inner and outer shells are spherical and that the surface brightness profiles of the Hα and He II λ4686 emission lines can be represented by those extracted along the East-West direction presented in Figure 1b and Figure 1d, the total flux corrected for reddening of these lines are 2.0×10^{-12} and >1.8×10^{-14} erg cm^{-2} s^{-1}, respectively. For the reddening correction, the extinction correction derived for the outer shell from the Hα to Hβ line ratio (c(Hβ)=1.1) was applied. Since the extinction towards the inner shell might be larger, as suggested by an Hα/Hβ line ratio larger than that of the outer shell, although based on an uncertain estimate of the Hβ and Hα fluxes of the inner shell, the He II flux of this shell should be regarded as a lower limit.

By adopting a distance to HuBi 1 of 5.3 Kpc[25], the Hα and He II λ4686 Å fluxes imply luminosities of $L_{\text{H}\alpha} = 7.0 \times 10^{33}$ erg s^{-1} and $L_{\text{He II } \lambda4686} \geq 6.2 \times 10^{31}$ erg s^{-1}. The corresponding H I and He II ionizing photon fluxes are $\log Q(\text{H I}) = 45.7$ and $\log Q(\text{He II}) \geq 43.8$, respectively. These ionizing fluxes can be compared to the output predicted by our non-LTE best-fit model to the spectrum of the CSPN. For the 1996 spectrum of the CSPN, this model predicts $\log Q(\text{He II}) = 34.3$, much smaller than the value derived from the observed He II lines. This same model predicts $\log Q(\text{H I}) = 48$, but the 2017 spectrum suggests that the H I ionizing flux has declined at least 4 orders of magnitude to $\log Q(\text{H I}) \approx 44$, also below the observed H I ionizing flux.

Spectro-photometric evolution of IRAS 17514. May 1991[4], July 1996 INT IDS, and July 2014 and May 2017 NOT ALFOSC optical spectra have been used, in conjunction with the original March 1989 BVR photometric data[3] and January 1971 USNO B-1 Catalog BR magnitudes[26], to investigate the spectro-photometric time evolution of IRAS 17514. The different spectra and photometric magnitudes are plotted in Figure 2b. The observed flux in each spectra has been corrected from the seeing and slit-width, although this correction is small, of a few percent. These spectra have also been used to fit a stellar continuum and determine the BVR magnitudes of the central star at each epoch. The time evolution of the flux of the star at different photometric bands is plotted in Figure 2a.

11
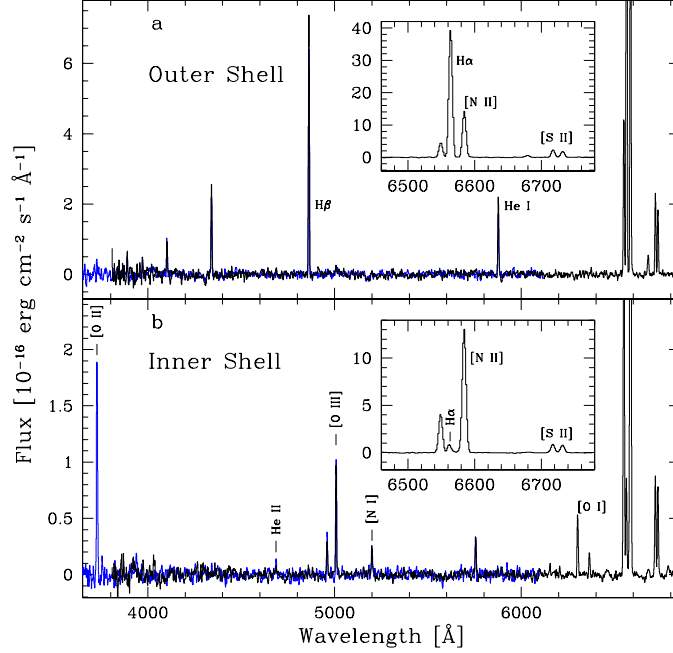
Supplementary Figure 3.– NOT ALFOSC grism #7 (black) and #14 (blue) spectra of the outer (a) and inner (b) shells of HuBi 1. The insets show the spectral range including the Hα, [N II] λλ6548,6584, and [S II] λλ6717,6731 emission lines. Note the singular detection of the He II λ4686 emission line in the inner shell.

Spectral models of the inner and outer shells of HuBi 1. The NOT ALFOSC two-dimensional spectra were also used to extract one-dimensional spectra of the inner and outer shells of HuBi 1 (Supplementary Figure 3), using the apertures shown in panels *b*, *c*, and *d* of Figure 1. A region of radius $0\rlap{.}{''}7$ at the location of the central star was excluded to excise its emission from the spectrum of the inner shell.

The outer shell is dominated by H I and He I recombination lines, with much fainter [N II] λλ6548,6584 and [S II] λλ6716,6731, and no [O II] λ3727 nor [O III] λλ4959,5007 emission lines. The density-sensitive [S II] λλ6716,6731 doublet has been used to derive an electronic density $\approx$200 cm^{-3}. At the distance of HuBi 1 and adopting a volume filling factor of 0.3[25], this density implies an ionized mass of 0.08 $M_{\odot}$, which is reasonable value for a PN. The code MAPPINGS V 5.1.13[27] was used to explore the evolution of the intensity of various emission lines in a freely cooling gas. The Supplementary Figure 4 shows the time-evolution of the electronic temperature, ionization fraction of hydrogen, and emissivity of several emission lines for a spherical photo-ionized cloud of gas once the ionizing source is switched off and the gas is allowed to cool freely. The abundances have been assumed to be solar and the electron temperature to be 10,000 K. The electron

12
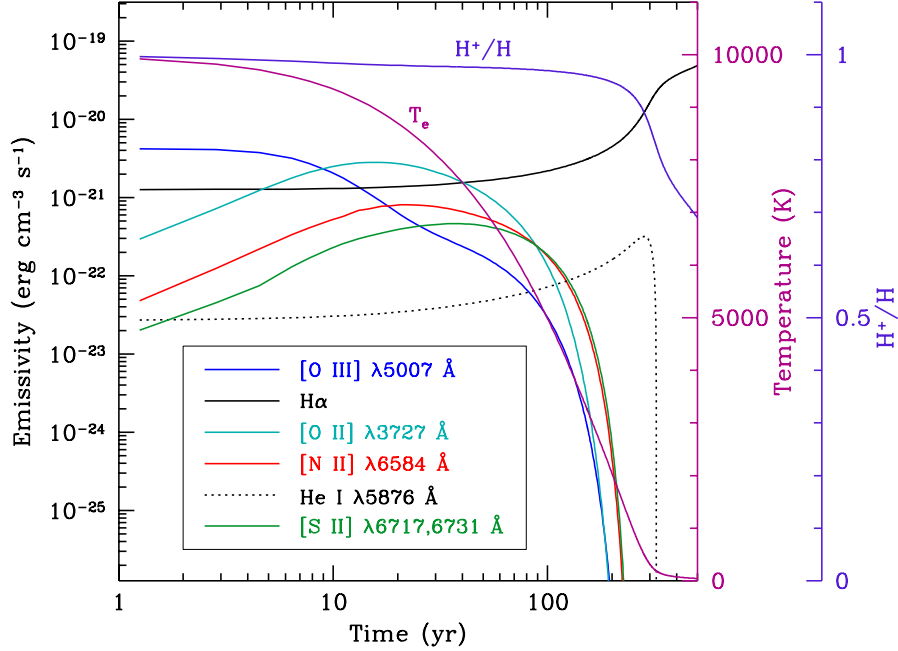
Supplementary Figure 4.– Time-evolution of the electron temperature T_e, hydrogen ionization fraction H$^+$/H, and emissivity of the Hβ, He I λ5876, [O II] λ3727, [O III] λ5007, [N II] λ6584, and [S II] $\lambda\lambda$6716,6731 emission lines of a photo-ionized cloud of gas with solar abundances, electron density of 200 cm^{-3} and electron temperature of 10,000 K after the ionizing source is switched off at time t=0.

density in the model is 200 cm^{-3}, as derived from the density-sensitive [S II] $\lambda\lambda$6717,6731 doublet line ratio. As time goes by, O^{++}, the most efficient coolant, is the first ion to fully recombine, followed by O$^+$, and then by N$^+$ and S$^+$. It takes longer for He$^+$ to recombine, whereas a significant fraction of hydrogen will remain ionized for a much longer period of time. The outer shell of HuBi 1 is found to be at the stage when the emissivities of the [N II] and [S II] emission lines are much higher than that of [O II]. In Supplementary Figure 4, this occurs between 90 and 220 years after the central source is switched off, but we note that, whereas the overall behavior of the gas remains the same, independently of the gas density (but for cases of extremely high metallicities), the time estimate may vary significantly depending on the metallicity of the gas and its density. The mild axisymmetry of the outer shell of HuBi 1 (see the description of the morpho-kinematical model) is not expected to affect significantly the main results presented here. Furthermore, these effects are certainly mitigated by the particular orientation of the long-slit, mostly orthogonal to the outer shell symmetry axis.

As for the inner shell, the brightest emission lines in its spectrum are those of [N II].

Fainter emission is detected in the forbidden lines of [O I], [O II], [O III], [N I], and [S II], as well as in the recombination emission lines of H I and He I, and the notable detection of the He II λ4686 emission line. The presence of high ionization lines in the inner shell, together with its intricate profile structure, can be attributed to shocks, as the central source is no longer capable to appreciably ionize the gas and produce He^{++}. To explore this possibility, we used also MAPPINGS to evaluate a shock expanding through a fully ionized (H^+/H=1, He^+/He=1) medium with solar abundances and a pre-shock density 200 cm^{-3}. The magnetic field was assumed to have a low value, $B_0 = 0 - 1\mu G$. Shocks with velocities above 50 km s^{-1} are required to produce [O III] emission, and above 70 km s^{-1} to produce the observed value of the He II/Hβ line ratio. Much higher shock velocities, above 100 km s^{-1}, can be firmly rejected as they imply line ratios very different from the ones observed. The emission structure behind a 70 km s^{-1} shock is qualitatively consistent with that observed in the inner shell of HuBi 1, with the He II emission peaking outside at the shock region and [N II] and [O III] peaking inside in the post-shock cooling region.

Low-mass Very Late Thermal Pulse Models. The evolved PN around IRAS 17514 and the strongly H-deficient composition of its stellar wind suggest a very late thermal pulse (VLTP) origin. In addition, the slow evolution of the central star implies a low-mass star. To test these assumptions, we computed several evolution sequences of VLTP events in low-mass stars using LPCODE, La Plata stellar evolution code. LPCODE is a one-dimensional stellar evolution code widely used for the computation of full evolutionary sequences from the zero age main sequence to the WD stage[29]. The last version of LPCODE has been carefully calibrated at different evolutionary stages to reproduce several AGB and post-AGB observables [30]. LPCODE has been successfully used to compute the evolution of post-AGB stars[30] and the formation of H-deficient stars through late helium flashes[31]

In order to create models of [WC] stars, we have adopted some low-mass AGB models previously computed[30] and adjusted the stellar winds during the last stage of the AGB evolution to ensure they left the AGB at the right time for a VLTP to take place in the post-AGB evolution of the sequence. The models correspond to initial masses 0.8 $M_\odot$ and 0.9 $M_\odot$ ($Z = 0.001$) and 1 $M_\odot$, 1.1 $M_\odot$, and 1.25 $M_\odot$ ($Z = 0.01$). The evolution of these sequences in the HR diagram is shown in the left panels of the Supplementary Figure 5, together with our luminosity and temperature determinations for IRAS 17514. The location of IRAS 17514 is consistent with a post-VLTP stage in all sequences. The surface abundances predicted for these VLTP models are shown in Table 1, together with our determinations for the surface abundances of IRAS 17514. The qualitative agreement between the abundances measured in IRAS 17514 and the predictions of VLTP computations is remarkable, supporting a VLTP event in IRAS 17514.

These models should also reproduce the time behavior of IRAS 17514. For this purpose, we
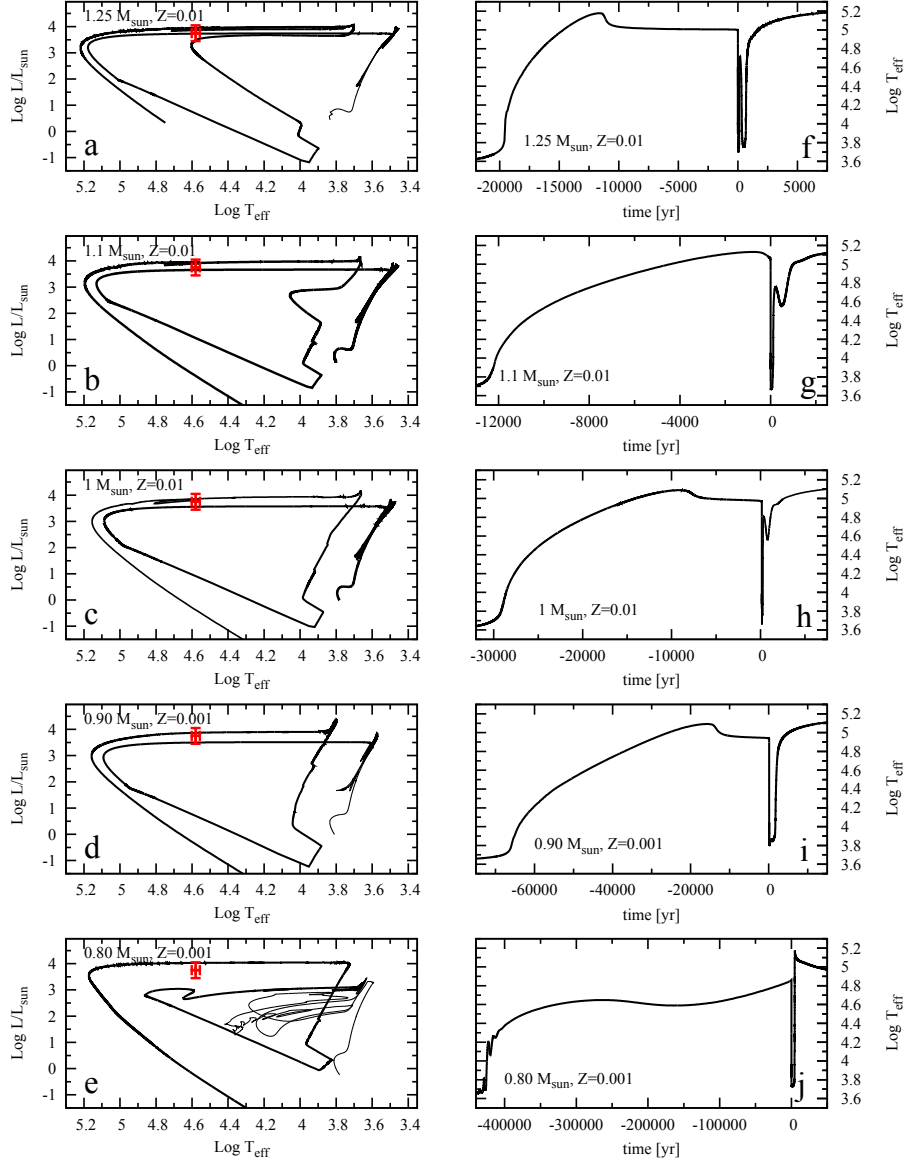
Supplementary Figure 5.– VLTP sequences of low-mass stars. (left) Evolution of the stellar sequences in the HR diagram, where the red-cross indicates the location of the central star of HuBi 1 with uncertainties as inferred from our best-fit non-LTE model (see the details of the non-LTE model fit). (right) Effective temperature evolution of the same sequences during the departure from the AGB and after the VLTP event (set at t=0).

show in the right panels of the Supplementary Figure 5 the time evolution of T_{eff} from the departure from the AGB ($\log T_{eff} < 3.7$) to the beginning of the WD phase ($\log T_{eff} \sim 5$)

Table 1.– Chemical abundances of IRAS 17514 and those of several VLTP sequences.

| Initial Mass	H	^{4}He	^{12}C	^{13}C	^{14}N	^{16}O	^{20}Ne	^{22}Ne
IRAS 17514	0.01–0.05	0.33±0.10	0.50±0.10		0.01	0.1	0.04	
0.8 $M_\odot$	0.030	0.52	0.30	0.041	0.016	0.086	9×10^{-5}	1×10^{-3}
0.9 $M_\odot$	5×10^{-3}	0.48	0.29	0.069	0.065	0.091	9×10^{-5}	9×10^{-4}
1.0 $M_\odot$	5×10^{-5}	0.40	0.34	0.074	0.056	0.116	9×10^{-4}	0.01
1.1 $M_\odot$	5×10^{-3}	0.38	0.37	0.059	0.028	0.145	9×10^{-4}	0.01
1.25 $M_\odot$	5×10^{-6}	0.41	0.33	0.067	0.047	0.133	9×10^{-4}	0.01

and through the VLTP event (chosen as t=0). The low density and morphological appearance of HuBi 1 suggest it is an evolved PN, which is further supported by its kinematical age $\approx$9,000 yr. On the other hand, the outer nebula is recombining, indicating that the ionizing source faded 90-220 years ago, whereas spectroscopic observations of IRAS 17514 show that its temperature has stayed almost constant at $T_\star \simeq 38,000$ K for at least two decades.

The 0.8 $M_\odot$ and 0.9 $M_\odot$ sequences take $\approx$400,000 and $\approx$60,000 years, respectively, between the departure from the AGB and the VLTP event, which is inconsistent with the estimated age of HuBi 1 (and even with the accepted visibility lifetime of PNe, $\approx$20,000 yr). Consequently, the evolution before the VLTP event can be used to reject very low-mass VLTP events. On the contrary, the time between the departure from the AGB and the point of maximum T_{eff} of the 1.0 $M_\odot$, 1.1 $M_\odot$, and 1.25 $M_\odot$ sequences is still below the accepted visibility lifetimes of PNe.

After the VLTP event, the 1.25 $M_\odot$ sequence stays as a born-again AGB giant for about 100 yr, then it reheats to 38,000 K, makes a double loop, crosses T_{eff} at 38,000 K again, stays as a giant for $\approx$150 years, and about 700 years after the star reheats back to 38,000 K. This sequence stays within the $T_{eff} \simeq 36,000-40,000$ K range for only 1, 7, and 5 years in each crossing, respectively, and thus it does not reproduce the observed spectral behavior of IRAS 17514 between 1989 and 2017. As for the 1.0 $M_\odot$ sequence, it is able to describe the behavior of IRAS 17514 in this period of time, as well as the existence of an old evolved PN, but the time-lapse between the departure from the AGB and the VLTP event for our 1.0 $M_\odot$ sequence cannot be shortened below $\simeq$22,000 years, resulting in a disagreement of a factor of two with the inferred kinematical age of the PN. Therefore, the VLTP evolution can be used to reject the 1.0 $M_\odot$ and 1.25 $M_\odot$ sequences, with the 1.1 $M_\odot$ sequence being the only one capable to reproduce accurately the time behavior of IRAS 17514 and its nebula.

As shown in Figure 3, the 1.1 $M_\odot$ sequence departs from the AGB about $\approx$12,000 yr before the occurrence of the VLTP event, in reasonable agreement with the kinematical

16
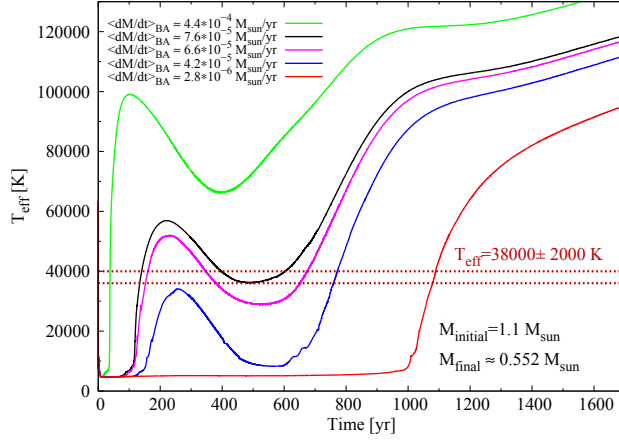
Supplementary Figure 6.– Predicted T_{eff} evolution of our 1.1 M$_\odot$ sequence after the VLTP event under different assumptions of the mass-loss rate through winds during the born-again AGB phase. The legend indicates the mean envelope mass removed per year at $\log T_{eff} < 3.8$.

age of HuBi 1. We note, however, that the post-VLTP evolution depends on the details of the mass removed by the stellar winds during the return to the AGB as a H-deficient giant (i.e., the Born Again AGB phase), which is very uncertain. Observations of bona fide VLTP events (V605 Aql, V4334 Sgr) indicate very high mass-loss rates, in the range $10^{-3} - 10^{-5} M_\odot$ yr^{-1}[2, 32], once the star becomes a cold AGB giant[1] ($\log T_{eff} < 3.8$). Consequently, we performed simulations of the post-VLTP evolution of our 1.1 M$_\odot$ sequence under different assumptions for the mass removed at $\log T_{eff} < 3.8$ during this phase. The Supplementary Figure 6 shows the details of such simulations. In particular, a mean mass-loss rate of $7.6\times10^{-5} M_\odot$ yr^{-1}, i.e., within the observed range in other born-again events, allows us to reproduce the observed behavior of IRAS 17514 between 1989 and 2017. The mass of the post-AGB star before the VLTP event is 0.551 $M_\odot$ and the total mass ejected amounts to 8×10^{-4} $M_\odot$.

The time evolution of this sequence is shown in Figure 3. This sequence matches most observed properties of HuBi 1 and its central star. It explains the existence of an old PN with kinematical age $\approx$9,000 yr, and the almost constant temperature $T_\star = 38000 \pm 2000$ K of the CSPN in the period of time between 1996 and 2014, its chemical enrichment, and its stellar luminosity $\log(L/L_\odot) = 3.75 \pm 0.3$.

Acnowledgements

Author Contribution.

M.A.G. planned the research project, programmed the observations, wrote the main body of the manuscript, and organized the writing of some subsections. A.A. performed the MAPPINGS simulations, C.M. the CLOUDY ones, and both devised the excitation nature of the inner and outer shells. C.K. estimated the ionizing flux necessary for the inner and outer shells. G.R.-L. reduced the imaging data and contributed to the analysis of the time-evolution of the central star. H.T. analised the spectrum of the central star using PoWR to determine its stellar parameters and abundances. L.S. and G.R.-L. obtained and reduced the high-dispersion spectroscopic observations, and together with L.F.M. and S.A.Z. analysed them using SHAPE. M.M.M.B. devised the post-AGB evolutionary scenario and computed the LPCODE VLTP evolutionary sequences. X.F. reduced the spectroscopic data and carried out the analysis of one-dimensional spectra and spatial profiles of emission lines. All authors contributed to the discussion of the different sections of this work.

Data and code availability.

The data that support the plots and other findings in this paper are available from the corresponding author on a reasonable request. CLOUDY, MAPPINGS and SHAPE can be freely downloaded from https://www.nublado.org, https://mappings.anu.edu.au/code and http://www.astrosen.unam.mx/shape/index.html, respectively. The LPCODE and PoWR codes used in this paper are similarly available under request from M.M. Miller Bertolami and H. Todt, respectively.

References

[1] Duerbeck, H. W. et al. The Rise and Fall of V4334 Sagittarii (Sakurai's Object). *Astron. J.* **119**, 2360–2475 (2000).

[2] Hajduk, M. et al. The Real-Time Stellar Evolution of Sakurai's Object. *Science* **308**, 231–233, (2005).

[3] Hu, J. Y., & Bibo, E. A. Discovery of a new cool WR star in a low excitation planetary nebula. *Astron. Astrophys.* **234**, 435–438 (1990).

[4] Pollacco, D. L., & Hill, P. W. The Planetary Nebula Surrounding the WC 11 Star IRAS 17514–1555. *Mon. Not. R. Astron. Soc.* **267**, 692–696 (1994).

[5] Hamann, W.-R. Wolf-Rayet stars of high and low mass, in *H*ydrogen Deficient Stars (eds. Jeffery, C.S., & Heber, U.) 127 (Astron. Soc. Pacif. Conf. Ser. Vol. 96, 1996).

[6] Peña, M. The Low Excitation Planetary Nebulae HuDo 1 and HuBi 1 and their [WC10] Central Stars. *Rev. Mex. Astron. Astrophys.* **41**, 423-433 (2005).

[7] Leuenhagen, U., & Hamann, W.-R. Spectral analyses of late-type [WC] central stars of planetary nebulae: more empirical constraints for their evolutionary status. *Astron. Astrophys.* **330**, 265–276 (1998)

[8] Corradi, R. L. M., Schönberner, D., Steffen, M., & Perinotto, M. Ionized haloes in planetary nebulae: new discoveries, literature compilation and basic statistical properties. *Mon. Not. R. Astron. Soc.* **340**, 417–446 (2003).

[9] Draine, B. T., & McKee, C. F. Theory of interstellar shocks. *Ann. Rev. Astron. Astrop.* **31**, 373–432 (1993).

[10] Perea-Calderón, J. V., García-Hernández, D. A., García-Lario, P., Szczerba, R., & Bobrowsky, M. The mixed chemistry phenomenon in Galactic Bulge PNe. *Astron. Astrophys.* **495**, L5-L8 (2009).

[11] Naito, H. et al. Five-year optical and near-infrared observations of the extremely slow nova V1280 Scorpii. *Astron. Astrophys.* **543**, A86 (2012).

[12] Clayton, G. C. The R Coronae Borealis Stars. *Pub. Astron. Soc. Pacif.* **108**, 225–241 (1996).

[13] Williams, P. M. Dust formation around WC stars, in *Wolf-Rayet Stars: Binaries; Colliding Winds; Evolution* (eds. K.A. van der Hucht & P.M. Williams) 335 (International Astronomical Union, IAU Symp. 163, Kluwer Academic Publishers, Dorcrecht, 1995).

[14] Williams, P. M. Eclipses and dust formation by WC9 type Wolf-Rayet stars. *Mon. Not. R. Astron. Soc.* **445**, 1253–1260 (2014).

[15] Acker, A., & Neiner, C. Quantitative classification of WR nuclei of planetary nebulae. *Astron. Astrophys.* **403**, 659–673 (2003).

[16] Blöcker, T. Evolution on the AGB and beyond: on the formation of H-deficient post-AGB stars. *Astrop. Sp. Sci.* **275**, 1–14 (2001).

[17] Schönberner, D. Asymptotic giant branch evolution with steady mass loss. *Astron. Astrophys.* **79**, 108–114 (1979).

[18] Zijlstra, A. A. The infrared [WC] stars. *Astrop. Sp. Sci.* **275**, 79–90 (2001).

[19] Acker, A., Gesicki, K., Grosdidier, Y., & Durand, S. Turbulent planetary nebulae around [WC]-type stars. *Astron. Astrophys.* **384**, 620–628 (2002).

[20] García-Rojas, J. et al. Analysis of chemical abundances in planetary nebulae with [WC] central stars. II. Chemical abundances and the abundance discrepancy factor. *Astron. Astrophys.* **558**, A122 (2013).

[21] Gesicki, K., Zijlstra, A.A., & Miller Bertolami, M.M. The mysterious age invariance of the planetary nebula luminosity function bright cut-off. *Nat. Astron.* (2018).

[22] Hamann, W.-R., & Gräfener, G. Grids of model spectra for WN stars, ready for use. *Astron. Astrophys.* **427**, 697–704 (2004).

[23] Hainich, R. et al. Wolf-Rayet stars in the Small Magellanic Cloud. I. Analysis of the single WN stars. *Astron. Astrophys.* **581**, A21 (2015).

[24] Reindl, N. et al. The rapid evolution of the exciting star of the Stingray nebula. *Astron. Astrophys.* **565**, A40 (2014).

[25] Frew, D. J., Parker, Q. A., & Bojičić, I. S. The Hα surface brightness-radius relation: a robust statistical distance indicator for planetary nebulae. *Mon. Not. R. Astron. Soc.* **455**, 1459–1488 (2016).

[26] Monet, D. G. et al. The USNO-B Catalog. *Astron. J.* **125**, 984–993 (2003).

[27] Sutherland, R. S., & Dopita, M. A. Effects of Preionization in Radiative Shocks. I. Self-consistent Models. *Astrophys. J. Sup. Ser.* **229**, 34 (2017).

[28] Steffen, W. et al. Shape: A 3D Modeling Tool for Astrophysics. *IEEE Transactions on Visualization and Computer Graphics* **17**, 454-465 (2011).

[29] Althaus, L.G. et al. The formation and evolution of hydrogen-deficient post-AGB white dwarfs: The emerging chemical profile and the expectations for the PG 1159-DB-DQ evolutionary connection. *Astron. Astrophys.* **435**, 631–648 (2005).

[30] Miller Bertolami, M.M. New models for the evolution of post-asymptotic giant branch stars and central stars of planetary nebulae. *Astron. Astrophys.* **588**, A25 (2016).

[31] Battich, T., Miller Bertolami, M.M., Córsico, A., & Althaus, L.G. Pulsational instabilities driven by the ϵ mechanism in hot pre-horizontal branch stars I. The Hot-Flasher Scenario. *Astron. Astrophys.* **in press**, arXiv:1801.07287 (2018).

[32] Clayton, G. C. et al. Evolution of the 1919 Ejecta of V605 Aquilae. *Astrophys. J.* **771**, 130 (2013).